Katoite under Pressure: An Ab initio Investigation of its Structural, Elastic and Vibrational Properties Sheds Light on the Phase Transition.

A. Erba, A. M. Navarrete-Lopez, V. Lacivita, Ph. D'Arco, C. M. Zicovich-Wilson
Katoite under Pressure: An Ab initio Investigation of its Structural, Elastic and Vibrational Properties Sheds Light on the Phase Transition.
PHYSICAL CHEMISTRY CHEMICAL PHYSICS (2015) 17

Katoite under Pressure: An Ab initio Investigation of its Structural, Elastic and Vibrational Properties Sheds Light on the Phase Transition.

Alessandro Erba,[a,*] Alejandra M. Navarrete-López,[a,b] Valentina Lacivita,[c,d] Philippe D'Arco[d,e] and Claudio M. Zicovich-Wilson[b]

Received Xth XXXXXXXXXX 20XX, Accepted Xth XXXXXXXXX 20XX
First published on the web Xth XXXXXXXXXX 20XX
DOI: 10.1039/b000000x

The evolution up to 65 GPa of pressure of structural, elastic and vibrational properties of the katoite hydrogarnet, $Ca_3Al_2(OH)_{12}$, are investigated with an *ab initio* simulation performed at the B3LYP level of theory, by using all-electron basis sets with the CRYSTAL periodic program. The high-symmetry $Ia3d$ phase of katoite, stable at ambient conditions, is shown to be destabilized, as pressure increases, by interactions involving hydrogen atoms and their neighbors which weaken the hydrogen bonding network of the structure. The corresponding thermodynamical instability is revealed by anomalous deviations from regularity of its elastic constants and by numerous imaginary phonon frequencies, up to 50 GPa. Interestingly, as pressure is further increased above 50 GPa, the $Ia3d$ structure is shown to become stable again (all positive phonon frequencies and regular elastic constants). However, present calculations suggest that, above about 15 GPa and up to at least 65 GPa, a phase of $I\bar{4}3d$ symmetry (a non-centrosymmetric subgroup of $Ia3d$) becomes more stable than the $Ia3d$ one, being characterized by strengthened hydrogen bonds. At low-pressures (between about 5 GPa and 15 GPa), both phases show some instabilities (more so for $I\bar{4}3d$ than for $Ia3d$), thus suggesting either the existence of a third phase or a possible phase transition of second order.

1 Introduction

In the last decades, a lot of attention has been devoted to the understanding of the incorporation of hydrogen into nominally anhydrous minerals (NAM) because of the remarkable effect it has on their technological and geophysical properties.[1–7] In particular, NAMs are of great geological interest in that they may potentially introduce large amount of "water" in the Earth mantle thus significantly modifying its elastic properties.[8–10] In this respect, garnets are among the most interesting candidates as possible hydrogen storage media for the Earth's mantle, given their abundance and stability.[11,12]

The hydrogarnet substitution ($SiO_4 \leftrightarrow O_4H_4$) in grossular has received special attention in that it represents an effective mechanism for including hydrogen into silicate garnets.[11,13–21] Hydrogrossular can be represented by the general formula $Ca_3Al_2(SiO_4)_{3-x}(OH)_{4x}$; when $0 < x < 1.5$ it is called hibschite and when $1.5 < x < 3$ it is called katoite.[19] At low temperature, there is complete solid solubility of the two end-members (grossular and silicon-free katoite; see Figure 1 for a graphical representation of the structure of the two systems). Hydrogarnets are known to be stable over the whole Earth's mantle pressure range;[9] natural hydrogarnets equilibrated at 180 km depth have been characterized.[10] In what follows, katoite will be used as a shortcut for silicon-free katoite. The characterization of the structural and mechanical properties of katoite under pressure is crucial for discussing its possible role as a major "water" reservoir in the Earth's mantle. This investigation has some implications of even broader general interest as it implies the full characterization of the evolution under pressure of hydrogen bonding in such a NAM that, as we are going to recall in a moment, is rather controversial, indeed.

Two distinct compression mechanisms are possible for garnets: bond shortening and bond bending.[12,22] A pioneering neutron powder diffraction study by Lager and Von Dreele in 1996 of katoite under pressure, up to 9 GPa, seemed to suggest a compression mechanism based on a cooperative rotation of corner-sharing tetrahedra and octahedra, similar to that observed for andradite.[15] Nonetheless, more recent measure-

[a] *Dipartimento di Chimica and Centre of Excellence Nanostructured Interfaces and Surfaces (NIS), Università di Torino, via Giuria 5, IT-10125 Torino, Italy. E-mail: alessandro.erba@unito.it*
[b] *Facultad de Ciencias, Universidad Autónoma del Estado de Morelos, Av. Universidad, 1001, Col. Chamilpa, 62209 Cuernavaca (Morelos), Mexico*
[c] *Sorbonne Universités, UPMC Univ Paris 06, Institut Calcul et Simulation (ICS), 4 place Jussieu, F-75005, Paris, France. Tel: +33 1 44 27 51 67.*
[d] *Sorbonne Universités, UPMC Univ Paris 06, UMR 7193, Institut des Sciences de la Terre Paris (ISTeP), 4 place Jussieu, F-75005 Paris, France.*
[e] *CNRS, UMR 7193, Institut des Sciences de la Terre Paris (ISTeP), 4 place Jussieu, F-75005 Paris, France.*

ments (an X-ray diffraction study up to 8 GPa by Lager *et al.* in 2002 and a neutron powder diffraction study up to 10 GPa by Lager *et al.* in 2005) showed that the compression is essentially driven by bond shortening rather than bond bending.[17,18] Three theoretical studies also confirmed this picture.[11,16,20]

A couple of major issues about the compressional behavior of katoite still remain unclear and require further analysis to be understood: i) the evolution of hydrogen bonding (*i.e.* of the related O−H and O···H distances) with pressure and ii) the nature of a possible phase transition of katoite under pressure which, till now, has only been suggested to occur, at about 5 GPa. In the next paragraphs we will summarize the main findings about these two open points.

As anticipated above, the description of the pressure dependence of hydrogen bonding in katoite is quite controversial. If experimental and theoretical studies all agree on the shortening of the O···H length with pressure, thus suggesting stronger hydrogen bonding interactions in the structure,[11,15–18,20] this is no more so for the O−H bond length. In this case, indeed, the first neutron diffraction study (Lager and Von Dreele, 1996) reported a significant shortening of that bond under pressure (with a contraction rate of about 0.012 Å/GPa up to 9 GPa) that seemed to be contradictory with the picture of strengthening hydrogen bonding,[15] whereas two theoretical studies, performed with a pure density-functional-theory (DFT) approach with pseudopotentials, reported in the year 2000 a slightly increasing bond length from ambient conditions (0.96 Å) up to 100 GPa (0.99 Å).[11,16] These findings stimulated Lager and co-workers to re-analyze their neutron diffraction data in 2002 by critically discussing the decreased resolution of their previous study above 2-3 GPa and by taking into account thermal motion effects; they concluded that the apparent shortening of the O−H bond could be explained in terms of an increasing thermal amplitude of hydrogen motion under increasing pressure. According to a simple riding model, they proposed a constant value of 0.94 Å in the entire pressure range explored.[17] A new and more accurate neutron diffraction study performed in 2005 up to 10 GPa, however, confirmed the O−H bond length shortening even if with a reduced rate with respect to the older one.[18] The authors still discussed a possible explanation in terms of thermal motion but admitted that the reason for an increasing mobility of hydrogen under pressure was not clear. A pressure-dependent positional disorder was also suggested as an alternative explanation.

In their X-ray diffraction study (2002), Lager *et al.* suggested a possible phase transition of katoite from its high-symmetry *Ia*3*d* space group to its $I\bar{4}3d$ non-centrosymmetric subgroup at about 5 GPa.[17] They proposed that H···H repulsion due to the compression of the inter-tetrahedral H···H distance might destabilize the original structure and drive the phase transition. The order parameter of such a transition

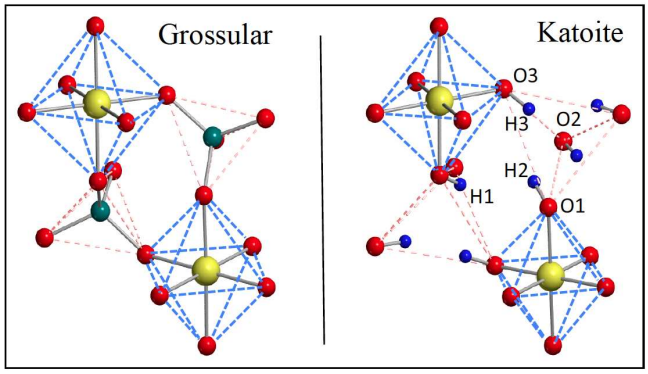

Fig. 1 (color online) Graphical representation of a portion of the structure of (left panel) grossular $Ca_3Al_2(SiO_4)_3$ and (right panel) katoite $Ca_3Al_2(OH)_{12}$. Octahedral, AlO_6, and tetrahedral, SiO_4 for grossular and $(OH)_4$ for katoite, subunits are highlighted with light blue and red dashed lines, respectively. Oxygens in red, silicons in green, aluminums in yellow, hydrogens in blue. Calcium atoms are not shown.

could be the shortening of the inter-tetrahedral H···H distance with respect to the intra-tetrahedral one. A further accurate determination of the positions of the hydrogens was required to corroborate the proposed model. In their neutron diffraction study of 2005, up to 10 GPa, however, they could not find such a crossing between inter- and intra-tetrahedral H···H distances, inter- remaining larger than intra- in the whole pressure range.[18] A couple of theoretical studies (Nobes *et al.*[11] and Pascale *et al.*[20]) could describe such a crossing (occurring at 8 GPa and 15 GPa, respectively) but were not able to detect any undoubtable sign of the occurrence of a phase transition.

In this study, we apply accurate *ab initio* simulations to the investigation of katoite under pressure, up to 65 GPa. The evolution with pressure of a number of different properties, such as structural, elastic and vibrational, is evaluated and discussed synergically. From the combined analysis of these properties, the behavior of the O−H bond length on compression is further characterized and strong evidences for the occurrence of a phase transition of katoite under pressure are reported.

A global hybrid functional, namely B3LYP,[23,24] is used in combination with all-electron atom-centered basis sets, which is known to accurately describe hydrogen bonding, as efficiently implemented into the periodic CRYSTAL14 program.[25,26] The description of the hydrogens is of course crucial for this system whose primitive cell contains 48 hydrogen atoms out of a total of 116 ones. In this respect, the present computational approach is expected to significantly improve the description with respect to previous computational studies where pure DFT functionals (much more affected by the self-interaction error) were used in combination with pseudopoten-

tials.[11,16]

The structure of the paper is as follows: in Section 2, the main computational techniques and parameters used for the calculations to be reported are illustrated, in particular as regards the evaluation of the pressure-volume relation, pressure-dependent elastic tensor, equation-of-state and vibration phonon frequencies; in Section 3, the evolution with pressure of structural, elastic and vibrational properties of katoite are investigated and its stability discussed; conclusions are drawn in Section 4.

2 Computational Methodology and Setup

The CRYSTAL14 program has been used for all the calculations reported in this study.[25] The B3LYP one-electron Hamiltonian is used, which contains a hybrid Hartree-Fock/Density-Functional exchange-correlation term. All-electron atom-centered Gaussian-type-function (GTF) basis sets are adopted. Oxygen, aluminum, calcium and hydrogen atoms are described by a 8-411G(d), 8-611G(d), 8-6511G(d) and 31G(p) contraction of primitive GTFs, respectively.

As implemented in the CRYSTAL program, infinite Coulomb and exchange sums are truncated according to five thresholds (here set to 7 7 7 7 16).[26] A sub-lattice is defined with a shrinking factor of 3 for sampling the reciprocal space, which implies 4 points in the irreducible Brillouin zone when katoite is in the $Ia\bar{3}d$ or $I\bar{4}3d$ space groups (they become 14 without any symmetry). Numerical integration techniques are used for the evaluation of the DFT exchange-correlation contribution (see the `XLGRID` keyword in the CRYSTAL User's Manual). The convergence of the self-consistent-field (SCF) step of the calculation is governed by a threshold on energy of 10^{-10} hartree.

Equilibrium and strained configurations are optimized by use of analytical energy gradients calculated with respect to both atomic coordinates and unit-cell parameters or atomic coordinates only, respectively.[27–29] A quasi-Newtonian technique is used, combined with the Broyden-Fletcher-Goldfarb-Shanno (BFGS) algorithm for Hessian updating.[30–33] Convergence is checked on both gradient components and nuclear displacements; the corresponding tolerances on their root mean square are chosen to be 10 times more severe than the default values for simple optimizations: 0.00003 a.u. and 0.00012 a.u., respectively.

2.1 Pressure-constrained Structure Optimization

A fully analytical scheme, based on the stress tensor, is used for optimizing the crystal volume under a given external pressure.[34] The stress tensor σ is a symmetric second-rank tensor that can be computed in terms of analytical energy gradients with respect to lattice parameters:

$$\sigma_{ij} = \frac{1}{V}\frac{\partial E}{\partial \varepsilon_{ij}} = \frac{1}{V}\sum_{k=1}^{3}\frac{\partial E}{\partial a'_{ki}}a_{kj}\ , \qquad (1)$$

with ε second-rank symmetric pure strain tensor and $i,j,k = x,y,z$. In the expression above, a_{ij} are elements of a 3×3 matrix, $\mathbf{A}$, where Cartesian components of the three lattice vectors $\mathbf{a}_1$, $\mathbf{a}_2$ and $\mathbf{a}_3$ are inserted by rows and V is the cell volume. When a distortion is applied to the cell, the lattice parameters transform as $a'_{ij} = \sum_{k=1}^{3}(\delta_{jk} + \varepsilon_{jk})a_{ik}$, where δ_{jk} is the Kronecker delta. By adding an external hydrostatic "pre-stress" $\sigma_{ij}^{\mathrm{pre}} = P\delta_{ij}$ to σ_{ij} and by inverting equation (1), one gets the expression for the constrained gradients

$$\frac{\partial H}{\partial a_{ij}} = \frac{\partial E}{\partial a_{ij}} + PV(\mathbf{A}^{-1})_{ji}\ . \qquad (2)$$

With the inclusion of a hydrostatic pressure, the function to be minimized becomes the enthalpy $H = E + PV$.[35] Let us stress that, at variance with the EOS approach (to be briefly described in Section 2.3), which is based on thermodynamical considerations, the enthalpy considered in constant-pressure optimizations does not correspond to the true function of state but rather to an approximation of it, as the internal energy term just corresponds to the mechanical electronic-nuclear energy without any statistical-mechanical contribution.

2.2 Elastic Tensor Calculation

If any finite pre-stress is absent, second-order elastic constants are simply defined as second energy density derivatives with respect to pairs of infinitesimal Eulerian strains:

$$C_{ijkl} = \frac{1}{V_0}\left(\frac{\partial^2 E}{\partial \varepsilon_{ij}\partial \varepsilon_{kl}}\right)_{\varepsilon=0}\ . \qquad (3)$$

An automated scheme for the calculation of the elastic tensor has been implemented in the CRYSTAL program,[36,37] that has been generalized also to low-dimensionality 1D and 2D systems.[38] Applications of this scheme cover a wide range of materials.[37,39–45]

When a finite pre-stress σ^{pre} is applied in the form of a hydrostatic pressure P, within the frame of finite Eulerian strain, the elastic stiffness constants become:[46–50]

$$B_{ijkl} = C_{ijkl} + \frac{P}{2}(2\delta_{ij}\delta_{kl} - \delta_{il}\delta_{jk} - \delta_{ik}\delta_{jl})\ , \qquad (4)$$

provided that V_0 in equation (3) is replaced by the equilibrium volume $V(P)$ at pressure P. A fully automated implementation in the CRYSTAL program of the calculation of the stiffness tensor $\mathbf{B}$ (and of $\mathbf{S} = \mathbf{B}^{-1}$, the compliance tensor) under pressure has recently been presented.[51,52] A two-index representation

of the elastic stiffness tensor is obtained ($B_{ijkl} \rightarrow B_{vu}$) by exploiting Voigt's notation, according to which $v,u = 1,\ldots,6$ (1 = *xx*, 2 = *yy*, 3 = *zz*, 4 = *yz*, 5 = *xz*, 6 = *xy*).[53] This tensor, in general, exhibits 21 independent elements that reduce to 3 (*i.e.* B_{11}, B_{12} and B_{44}) for crystals with cubic symmetry, as in the case of katoite. A number of elastic properties (such as bulk modulus, shear modulus, Young modulus, Poisson's ratio, etc.) can be deduced from the elastic constants.[53]

For the elastic constant calculation, four strained configurations are considered for each independent strain, with a dimensionless strain amplitude of 0.001 (*i.e.* 0.1 %). Larger strain amplitudes (about 1%, as generally adopted in these studies) have been tested but result in a wrong description of the elasticity of such a soft system where the numerical derivatives really need to be evaluated in the $\varepsilon \rightarrow 0$ limit. Numerical instabilities appear just for strain amplitudes below 0.02% for this system.

2.3 Equation of State Determination

An alternative approach for computing the bulk modulus and the $P-V$ relation of a crystalline material is via so-called Equations of State (EOS). "Cold" EOSs are energy-volume (or pressure-volume) analytical relations which describe the behavior of a solid under compression and expansion, at $T = 0$ K (that is the case of standard *ab initio* simulations) and are quite used in solid state physics and geophysics.[54,55]

Energy-volume data are numerically fitted to the analytical $E(V)$ functional form of the EOS. From $P = -\partial E/\partial V$, the *P-V* connection is established. The explicit dependence of the bulk modulus on volume (or pressure from *P-V*), is then given by $K(V) = V\partial^2 E/\partial V^2$. Within this approach, zero-point motion effects are generally neglected which are expected to reduce computed bulk moduli and increase computed equilibrium volumes.[56]

A number of universal EOS have been proposed so far.[54,57–62] All of them are phenomenological and can behave quite differently from each other as regards extrapolation at high pressure. Comprehensive reviews and comparisons of different EOSs are available in the literature.[63–67] Four EOSs are currently implemented in the CRYSTAL14 program (the full EOS calculation is activated by a single keyword):[51] the original third-order Murnaghan's,[57] the third-order Birch's,[58,59] the logarithmic Poirier-Tarantola's,[62] and the exponential Vinet's.[60]

2.4 Phonon Frequency Evaluation

Harmonic vibration frequencies at the Γ point (*i.e.* at the center of the first Brillouin zone in reciprocal space) are obtained from the diagonalization of the mass-weighted Hessian matrix of the second energy derivatives with respect to atomic displacements u:[68–71]

$$W^{\Gamma}_{ai,bj} = \frac{H^{\mathbf{0}}_{ai,bj}}{\sqrt{M_a M_b}} \quad \text{with} \quad H^{\mathbf{0}}_{ai,bj} = \left(\frac{\partial^2 E}{\partial u^{\mathbf{0}}_{ai} \partial u^{\mathbf{0}}_{bj}} \right) , \qquad (5)$$

where atoms a and b (with atomic masses M_a and M_b) in the reference cell, $\mathbf{0}$, are displaced along the i-th and j-th Cartesian directions, respectively.

In CRYSTAL, first derivatives of the total energy per cell ($v_{ai} = \partial E/\partial u_{ai}$) with respect to atomic displacements from the equilibrium configuration $\mathscr{R}^{\text{eq}}$ are computed analytically, whereas second derivatives numerically, using a two-point formula:

$$\frac{\partial^2 E}{\partial u_{ai} \partial u_{bj}} \approx \frac{v_{ai}(\mathscr{R}^{\text{eq}}, u_{bj} = +\overline{u}) - v_{ai}(\mathscr{R}^{\text{eq}}, u_{bj} = -\overline{u})}{2\overline{u}} ,$$

where $\overline{u}$ = 0.003 Å, a value 10 - 50 times smaller than that used in other solid state programs.[72–74]

3 Results and Discussion

3.1 Pressure-Volume Relation

Let us consider first the pressure-volume relation of $Ia3d$ katoite. At variance with previous theoretical studies[11,16,20] where the *P-V* relation was determined by fitting energy-volume data to the third-order Birch-Murnaghan equation-of-state, in this study pressure-constrained structure optimizations are performed. The procedure presented by Doll[34] and briefly recalled in Section 2.1 has been followed which is free of any possible interpolation/extrapolation issue. A total of 21 pressures have been considered, up to 60 GPa; for each of them, the $Ia3d$ cubic structure of katoite has been optimized by relaxing the lattice parameter and the atomic coordinates. The corresponding *P-V* relation, as computed at B3LYP level, is given in Figure 2, along with some experimental determinations: Olijnyk *et al.*[14] performed an X-ray diffraction experiment in 1991 up to 42 GPa (full circles), Lager and Von Dreele[15] a neutron diffraction study in 1996 up to 9 GPa (empty circles), Lager *et al.*[17] an X-ray diffraction study in 2002 up to 8 GPa (empty squares) and Lager *et al.*[18] a neutron diffraction study in 2005 up to 10 GPa (full squares).

Our computed data are found to agree better with the first experimental determination by Olijnyk *et al.*, where a wide pressure range was explored, than with more recent determinations where smaller pressure ranges have been considered. As a cross-check, we also computed the *P-V* relation with a standard EOS approach by interpolating energy-volume data in the whole range [0 GPa - 65 GPa], with the four expressions mentioned in Section 2.3: the agreement with our analytical stress tensor approach is remarkable in all cases, reflecting the

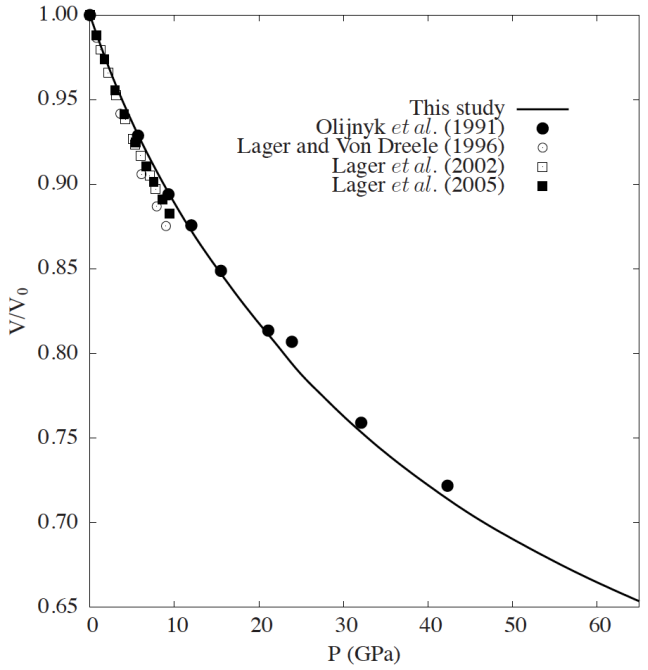

Fig. 2 Pressure-volume relation of katoite. The theoretical result, as obtained at B3LYP level with the analytical stress tensor approach presented in Section 2.1, is reported as continuous line. Experimental data are from Olijnyk *et al.*[14] (full circles), Lager and Von Dreele[15] (empty circles), Lager *et al.*[17] (empty squares) and Lager *et al.*[18] (full squares).

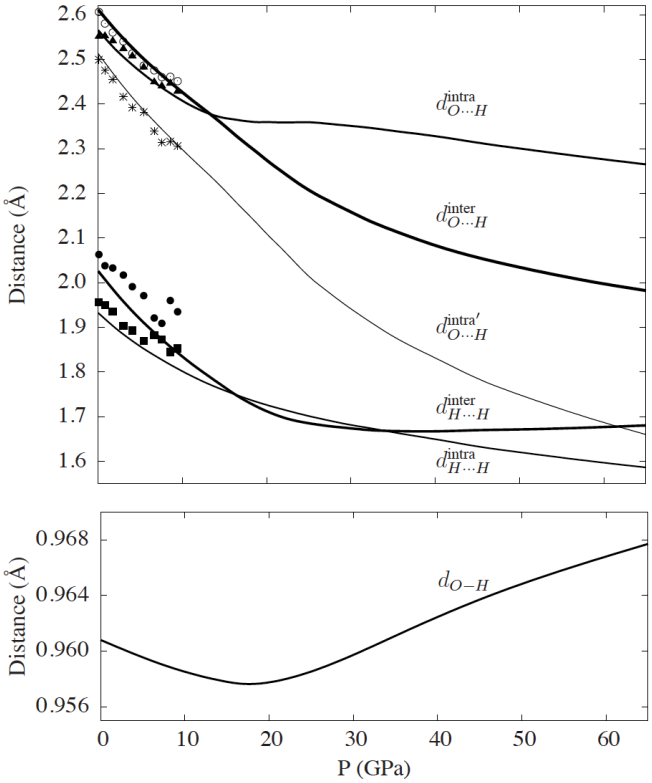

Fig. 3 Selected interatomic distances in *Ia*3*d* katoite, connected to the hydrogen bonding pattern of the structure, as a function of pressure, as computed in the present study (continuous lines). See text and Figure 1 for the definition of the distances. In the upper panel, experimental determinations by Lager *et al.*[18] are also reported for comparison.

accuracy of both implementations in the CRYSTAL program, which are based on radically different approaches. We will discuss the determination of the bulk modulus of katoite in Section 3.3.

In 2004, Pascale *et al.*[20] discussed in their *ab initio* study that no evidences of a pressure-induced phase transition in katoite can be found simply by starting from the *Ia*3*d* phase and performing geometry optimizations by removing symmetry, at this level of theory. This is essentially due to the fact that nuclear configurations corresponding to minima on the potential-energy-hypersurface (PEH) in the *Ia*3*d* symmetry still constitute zero-gradient critical points of the *P1* PEH thus preventing for further structural optimization. In order to overcome this numerical problem and reach lower energy nuclear configurations, one should run an optimization of the *P1* structure starting from a non-optimized geometry. Due to the high computational cost and arbitrariness in the selection of the starting configuration of such an optimization, we decided, instead, to perform phonon frequency calculations on the optimized cubic structure. With this procedure, non-equilibrium configurations are explicitly explored as atoms are displaced from their optimized positions. Lower energy nuclear configurations could then be reached (see Section 3.3 for more details).

3.2 Structural Characterization

As regards their structural modifications under pressure, aluminosilicate garnets are generally characterized by a certain degree of bond bending via corner-sharing polyhedral rotation.[12,22] Despite early evidences for a similar mechanism also for katoite,[15] it is now well-established from both experimental and theoretical studies that a bond shortening mechanism is occurring during compression in katoite.[11,16–18,20] For this reason, we restrict our attention on the description of the evolution under pressure of bond lengths and interatomic distances rather than of bond angles (that have been carefully described in a previous study[20] where the same computational approach has been used).

In Figure 3 we report, as a function of pressure up to 65 GPa, several interatomic distances which are of interest in the description of hydrogen bonding in katoite. In the lower panel, the O−H bond length (d_{O-H}) is reported. In the upper panel, two H···H distances are shown: the intra-tetrahedral

one, H2···H3 in Figure 1, ($d^{\text{intra}}_{H\cdots H}$), and the inter-tetrahedral one, H1···H2 in Figure 1, ($d^{\text{inter}}_{H\cdots H}$). Three O···H distances are also reported: one inter-tetrahedral, O1···H1 in Figure 1, ($d^{\text{inter}}_{O\cdots H}$), and two intra-tetrahedral, O3···H2 in Figure 1, ($d^{\text{intra}}_{O\cdots H}$), and O2···H2 in Figure 1, ($d^{\text{intra}'}_{O\cdots H}$). In the upper panel, experimental structural determinations from neutron diffraction measurements are also reported for comparison.[18]

As anticipated in the introduction, several experimental and theoretical studies agree on the shortening of the O···H lengths with pressure (see upper panel of Figure 3).[11,15–18,20] On the contrary, experimental and previous theoretical studies largely disagree on the description of the evolution under pressure of the d_{O-H} bond length. On the one hand, neutron diffraction experiments seem to suggest a strong shortening of the O−H bond as pressure increases up to about 10 GPa;[15,18] on the other hand, a couple of theoretical studies by Nobes *et al.*[11,16] reported an almost constant, slightly increasing, d_{O-H} up to 100 GPa.

In this study we find something significantly different from both previous suggestions and, as we will discuss in what follows, consistent with other structural and thermodynamical evidences of a phase transition under pressure. From inspection of the lower panel of Figure 3, indeed, it can be seen how hybrid *ab initio* simulations predict the d_{O-H} bond length of the *Ia*3*d* phase to shorten almost linearly from 0.961 Å at ambient pressure to 0.958 Å at about 18 GPa. In this pressure range, d_{O-H} decreases but with a slower rate with respect to the overall cell compression thus suggesting the development of hydrogen bonds. Above 18 GPa, the O−H bond length increases regularly, according to a picture where hydrogen bonds have become strong enough to prevail over the structural compression imposed by pressure.

A possible phase transition under pressure of katoite, at about 5 GPa, has been suggested by Lager and co-workers in their X-ray diffraction study in 2002. The authors suggested a mechanism of the transition according to which the increasing inter-tetrahedral H···H repulsion with pressure would destabilize the structure. In this respect, a crossing of $d^{\text{inter}}_{H\cdots H}$ and $d^{\text{intra}}_{H\cdots H}$ could be expected as pressure increases.[17] In their neutron diffraction study in 2005, however, Lager and co-workers were unable to find such a crossing up to 10 GPa (see their data as reported in the upper panel of Figure 3; full circles and squares).[18] As regards the H···H distances (upper panel of Figure 3), we find that at zero pressure the inter-tetrahedral distance is longer than the intra-tetrahedral one. With increasing pressure, $d^{\text{inter}}_{H\cdots H}$ shortens more quickly than $d^{\text{intra}}_{H\cdots H}$ until it becomes smaller at about 18 GPa. After this first crossing, $d^{\text{inter}}_{H\cdots H}$ becomes practically constant (even slightly increasing) while $d^{\text{intra}}_{H\cdots H}$ keeps shortening. As a consequence, a second crossing occurs at about 34 GPa.

So far, the concomitance, at 18 GPa, of the change in behavior of the d_{O-H} bond length and the crossing of $d^{\text{inter}}_{H\cdots H}$ and $d^{\text{intra}}_{H\cdots H}$, supports the model according to which interactions of hydrogen atoms with their neighbors may play a significant role in the structural adaptation of katoite under pressure. We shall now discuss the elastic and vibrational behavior of katoite under pressure. As we will see in the next section, its elastic and phonon characterization underpins the existence of a phase transition.

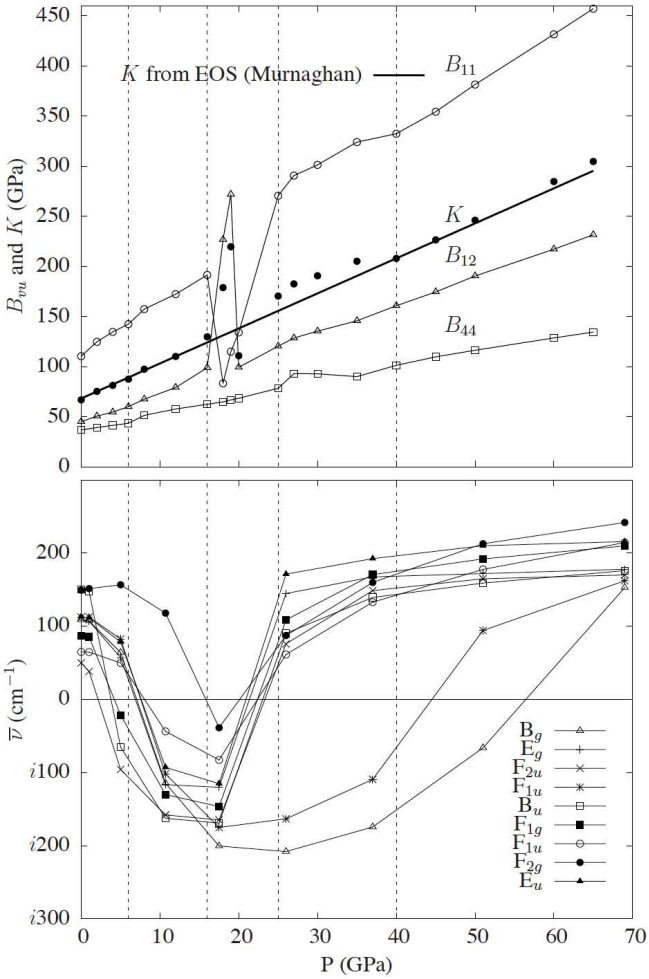

Fig. 4 Evolution with pressure of (upper panel) symmetry-independent elastic stiffness constants and bulk modulus and (lower panel) soft phonon wave-numbers of katoite constrained in the *Ia*3*d* space group. In the upper panel, the continuous line represent the bulk modulus obtained from the third-order Murnaghan EOS. Vertical dashed lines define pressure ranges discussed in the text.

3.3 Looking for the Phase Transition

In Section 3.1, we have discussed how, starting from the *Ia*3*d* phase of katoite, the existence of a pressure-induced phase

transition could not be predicted simply by performing standard geometry optimizations in which symmetry has been switched off. More sophisticated computational techniques are then necessary in order to investigate other physical properties somehow more sensitive to the phase transition. In what follows we will discuss how elastic constants and phonon frequencies can effectively come to the rescue in this respect.

Following the procedure described in Section 2.2, the elastic stiffness tensor **B** of *Ia*3*d* katoite has been fully characterized at 18 different pressures from 0 up to 65 GPa. The three symmetry-independent elastic stiffness constants, B_{11} (empty circles), B_{12} (empty triangles) and B_{44} (empty squares), are reported in the upper panel of Figure 4. The corresponding bulk modulus, $K = (B_{11} + 2B_{12})/3$, is reported at each pressure (full circles) and compared with that obtained by fitting energy-volume data to the third-order Murnaghan EOS (thick solid line). From inspection of the figure (*i.e.* from the analysis of the elastic response of katoite when constrained in the *Ia*3*d* space group), the explored pressure range can be subdivided into five regions (marked with vertical dashed lines): i) from 0 to 6 GPa, the three elastic constants vary regularly with pressure, the elastic bulk modulus is also regular and coincides with the one obtained from the EOS; ii) from 6 to 16 GPa, the B_{11} and B_{44} constants display small irregularities and the elastic bulk modulus only slightly deviates from its EOS counterpart; iii) from 16 to 25 GPa, we notice the dramatic softening of the B_{11} constant, the strengthening of the B_{12} constant and the corresponding strong deviations from regularity of the elastic bulk modulus, pointing to some unusual structural behavior that could be due to the imposed symmetry; iv) from 25 to 40 GPa, the *Ia*3*d* structure still shows deviations from regularity of the three elastic constants and of the bulk modulus, though to a lower extent with respect to the previous range; v) above 40 GPa, the three elastic constants show a nice regularity, the elastic bulk modulus becomes regular again and almost coincides with the EOS one. So far, we notice that the unusual elastic behavior of the *Ia*3*d* structure occurs in a pressure range where $d^{\text{inter}}_{H\cdots H}$ was shown to become shorter than $d^{\text{intra}}_{H\cdots H}$ (see Figure 3). This pressure range also includes the minimum in the d_{O-H} bond length.

Let us now analyze the evolution with pressure of phonon frequencies of the *Ia*3*d* phase of katoite, which have been computed at nine different compressions between 0 and almost 70 GPa. At each compression, the 348 phonon frequencies of katoite are computed, following the procedure described in Section 2.4, whose symmetry properties can be described in terms of the following partition of the reducible representation built on the basis of the Cartesian coordinates of the atoms in the cell:

$$\begin{aligned}\Gamma_{total} \;=\; & 6A_{1g} \oplus 7A_{2g} \oplus 13E_g \oplus 21F_{1g} \oplus 20F_{2g} \oplus 7A_{1u} \oplus \\ & 8A_{2u} \oplus 15E_u \oplus 24F_{1u} \oplus 23F_{2u}\,. \qquad (6)\end{aligned}$$

Table 1 Isotopic shifts $\Delta\nu$ of the nine unstable vibration modes of *Ia*3*d* katoite at P = 18 GPa when ^{44}Ca is substituted for ^{40}Ca, ^{29}Al for ^{27}Al, ^{18}O for ^{16}O and D for H. The imaginary frequencies of the 9 non-substituted modes are also reported along with the corresponding irreducible representation (irep).

irep	#	ν (cm^{-1})	$\Delta\nu$ (cm^{-1})			
			^{44}Ca	^{29}Al	^{18}O	D
B_g	1	*i*199.7	0.6	0.0	0.7	52.7
F_{1u}	2-4	*i*174.2	0.1	0.5	1.5	41.8
B_u	5	*i*167.4	0.0	0.0	1.4	37.4
F_{2u}	6-8	*i*163.6	0.5	0.9	1.5	39.7
F_{1g}	9-11	*i*145.0	0.2	0.0	1.9	35.1
E_g	12-13	*i*117.9	0.1	0.0	1.1	28.5
E_u	14-15	*i*113.6	0.1	0.7	1.2	26.2
F_{1u}	16-18	*i*81.6	0.4	0.2	2.0	13.1
F_{2g}	19-21	*i*33.8	0.0	0.0	0.4	8.5

The continuity of the vibration frequencies on volume has been determined by computing scalar products of the corresponding normal modes. Nine normal modes give imaginary frequencies at least for one of the considered pressures, thus indicating that the *Ia*3*d* phase is not a proper minimum of the lattice potential energy surface; the corresponding wave numbers are shown in the lower panel of Figure 4 as a function of pressure. From their analysis, one can see how the *Ia*3*d* phase, stable at very low pressures, becomes more and more unstable as pressure increases up to about 18 GPa where the maximum number of imaginary frequencies is found (*i.e.* all nine modes give imaginary frequencies at that pressure). As pressure is further increased, most of the unstable normal modes come rapidly back to positive phonon frequencies: above 25 GPa only two of them are still imaginary. Also these two modes are progressively coming back to the stability domain which they eventually rich above 55 GPa of pressure. This picture sheds light on the analysis of the elastic response discussed above.

If the hypothesis of an increasing repulsion between hydrogen atoms and their neighbors that destabilizes the *Ia*3*d* structure as a function of pressure is true, then these nine unstable modes (for a total of 21 imaginary frequencies) should be found to be dominated by the motions of the hydrogens. In order to characterize such modes, we have performed an isotopic shift analysis at P = 18 GPa (where they all give imaginary frequencies). Once the Hessian matrix has been computed, isotopic frequency shifts can be easily evaluated, at almost zero computational cost, by changing the atomic masses in equation (5). Four different isotopic substitutions have been explored: ^{44}Ca for ^{40}Ca, ^{29}Al for ^{27}Al, ^{18}O for ^{16}O and D for

Table 2 Selected elastic stiffness constants of katoite, computed as a function of pressure in the *P1* triclinic space group. The corresponding elastic bulk modulus K is also reported and compared with that obtained for the $Ia3d$ phase from the Murnaghan EOS, K_{EOS}. All data are in GPa.

P	B_{11}	B_{22}	B_{33}	B_{12}	B_{13}	B_{23}	K	K_{EOS}
2	127	128	131	46	47	46	74	75
6	155	155	155	59	59	59	91	90
16	204	204	204	89	89	89	127	125
18	236	237	239	90	92	94	139	132
20	223	219	215	100	99	99	140	139
27	261	261	261	120	120	120	166	162
40	306	306	306	161	161	161	209	208
60	418	418	418	218	218	218	284	278

H. The computed shifts $\Delta\nu$ are reported in Table 1 showing that Ca, Al and O atoms are scarcely involved in the collective atomic motions of these nine modes. On the contrary, they are significantly affected by the substitution of deuterium for hydrogen, with difference as large as 26 %, thus confirming that hydrogen atoms play a major role in such a structural instability.

3.4 An Insight into the New Phase

From the analysis of the evolution with pressure of elastic constants and phonon frequencies of the $Ia3d$ phase of katoite, clear evidences of a pressure-induced phase transition have been discussed in the previous section. In order to characterize the new phase, we perform an analysis of the symmetry features of the elastic stiffness tensor **B**, introduced in Section 2.2. To do so, we compute **B** at several pressures, by completely removing the symmetry of katoite (*i.e.* by imposing the *P1* space group). Depending on the particular symmetry of the lattice, indeed, the elastic tensor exhibits specific symmetry features. For a cubic lattice, three independent elastic constants are found ($B_{11} = B_{22} = B_{33}$, $B_{12} = B_{13} = B_{23}$ and $B_{44} = B_{55} = B_{66}$), the others being null by symmetry. For a triclinic crystal, all elements are independent and none of them is constrained to be zero by symmetry.

Selected elastic constants of katoite, as computed as a function of pressure in the triclinic *P1* space group, are reported in Table 2. The corresponding bulk modulus K is also reported and compared with that obtained for the $Ia3d$ phase from the Murnaghan EOS, K_{EOS}. Many elastic constants are not reported in the table; note that all the constants that would be zero by symmetry in cubic lattices are found to be numerically zero in the triclinic calculation. From inspection of the table, it can be seen how, within the numerical noise of the calculations, the computed elastic constants essentially show a cubic character in the whole pressure range: $B_{11} \approx B_{22} \approx B_{33}$ and $B_{12} \approx B_{13} \approx B_{23}$. This is particularly interesting in the $16 < P < 27$ range because can be considered as a strong evidence of the cubic character of the new phase. The bulk modulus K computed from the elastic constants is always very close to K_{EOS} while this was not the case for the elastic bulk modulus of the $Ia3d$ phase (see again Figure 4 in that pressure range).

Overall, from the analysis of the shape of the computed elastic tensor without any explicit symmetry-constraint, the cubic character of the new phase can be inferred. These findings seem to corroborate the proposed $I\bar{4}3d$ non-centrosymmetric subgroup of $Ia3d$ for the new phase, as suggested by Lager *et al.* in 2002.[17] As a final verification, we explicitly explore the behavior of this $I\bar{4}3d$ phase under compression; the last part of this section will be devoted to the presentation of the corresponding structural, elastic and vibrational properties which essentially confirm its stability above 15 GPa.

In Figure 5, the same structural, elastic and vibrational properties that we previously presented in Figures 3 and 4 for the $Ia3d$ phase, are reported for the $I\bar{4}3d$ phase of katoite as a function of pressure. Let us, first, discuss its thermodynamical stability by analyzing the evolution under pressure of its elastic and phonon properties. In the lowest panel of the figure, for each of the six considered pressures, the smallest vibration frequencies are reported.[75] We can clearly observe that: i) at $P = 0$, the $I\bar{4}3d$ phase is stable; ii) at variance with the high-symmetry $Ia3d$ phase, above 15 GPa all the vibration frequencies are positive thus confirming the stability of the $I\bar{4}3d$ phase (in particular in the 16 GPa $< P <$ 25 GPa range where the $Ia3d$ phase showed the maximum instability); iii) unexpectedly, in the 0 GPa $< P <$ 15 GPa pressure range, three imaginary frequencies (up to $i122$ cm^{-1}) are found which suggest a residual instability of the $I\bar{4}3d$ phase in the low-pressure regime. The analysis of its elastic response confirms this picture: above 15 GPa of pressure, the three symmetry-independent elastic stiffness constants (B_{11}, B_{12} and B_{44}) vary regularly with pressure, providing a linear elastic bulk modulus rather close to the EOS determination. At low pressures, these elastic constants show significant deviations, B_{11} and B_{44} softening and B_{12} strengthening.

In the two upper panels of Figure 5, the main interatomic distances related to the description of hydrogen bonding in katoite are reported. It is clearly seen that, above 15 GPa, one of the two symmetry-independent d_{O-H} bond lengths regularly increases with pressure, suggesting a systematic strengthening of the hydrogen bonds in the structure; the other one is almost independent of pressure. In the low-pressure regime, these O−H bonds show clear deviations from regularity which

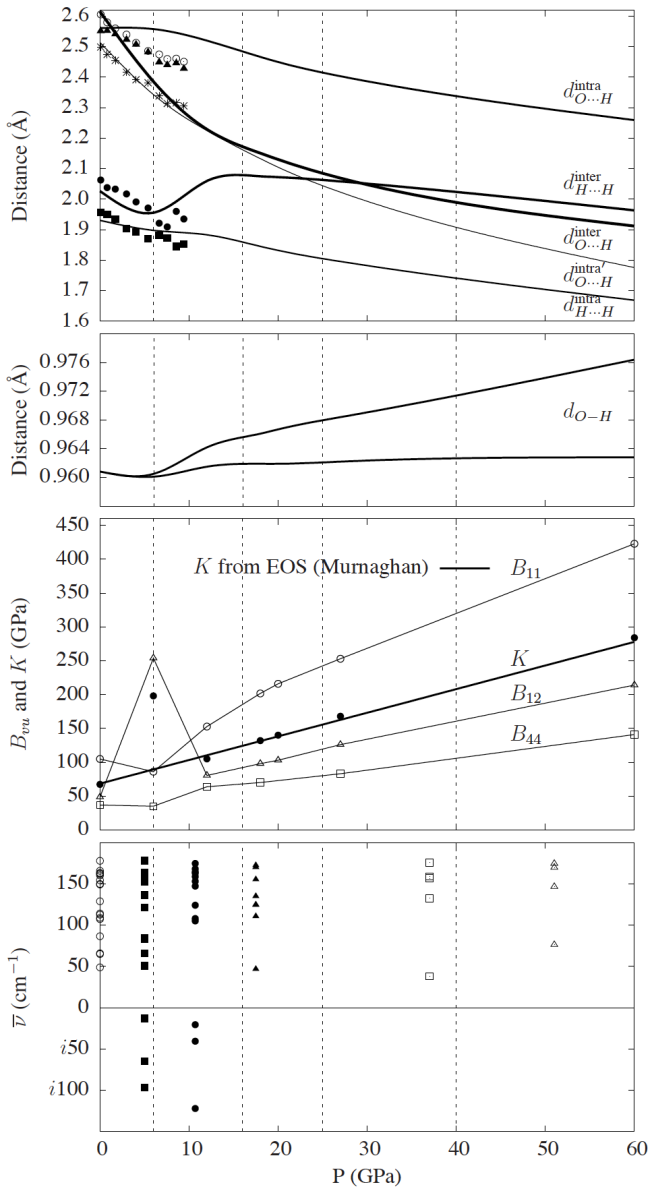

Fig. 5 Structural, elastic and vibrational properties of the $I\bar{4}3d$ phase of katoite as a function of pressure. See captions to Figures 3 and 4 for details. In the lowest panel, the smallest vibration frequencies are reported for each considered pressure.

can be related to the simultaneous variation of the H···H distances. Within this model (selected composition and $I\bar{4}3d$ symmetry), we could propose that destabilizing interactions arise from the short H···H inter-tetrahedral distance. In the $I\bar{4}3d$ phase, $d^{inter}_{H\cdots H}$ never becomes shorter than $d^{intra}_{H\cdots H}$ but shows a significant shortening at about 6 GPa (upper panel of the figure). The $I\bar{4}3d$ phase of katoite is then found to be thermodynamically more stable than the $Ia3d$ one above ap-

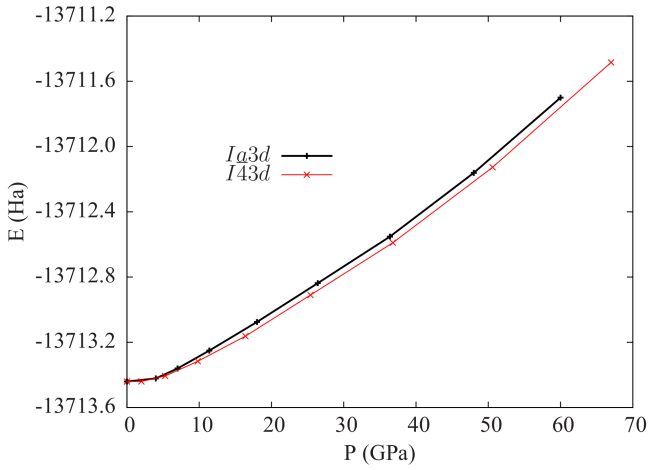

Fig. 6 (color online) Pressure dependence of the total energy per primitive cell of $Ia3d$ (black line) and $I\bar{4}3d$ (red line) katoite.

proximately 15 GPa (as Figure 6 confirms). At low-pressures (below approximately 5 GPa), the high-symmetry $Ia3d$ phase is the most stable while in the intermediate 5 GPa $< P <$ 15 GPa pressure range both of them are found to be unstable ($I\bar{4}3d$ more so than $Ia3d$). In that pressure range, our calculations seem to suggest either the existence of a third different phase or the possible coexistence of both phases, according to a second-order transition.

4 Conclusions

The behavior of the katoite hydrogarnet, $Ca_3Al_2(OH)_{12}$, under pressures up to 65 GPa, has been investigated theoretically by means of *ab initio* simulations, performed at the B3LYP level of theory, using all-electron Gaussian-type orbital basis sets and the CRYSTAL program. Many of the controversial aspects related to the evolution of hydrogen bonding with pressure and a possible pressure-induced phase transition have been rationalized.

The response to external pressure of its structural, elastic and vibrational phonon properties is fully characterized by combining together many complex algorithms which demand high performance computational resources for a system containing 116 atoms per primitive cell.[76] The presented results show a different degree of sensitivity to pressure-induced thermodynamic instability of different computed quantities which can prove extremely useful for further characterizations of phase transitions of hydrogarnets: phonon frequencies $\geq$ elastic constants $>$ structural features $\gg$ equation-of-state.

The high-symmetry $Ia3d$ phase of katoite, stable at ambient conditions and up to about 5 GPa, is found to be destabilized under increasing pressure and hydrogen atoms are found

to play a major role in this structural instability. The maximum instability is observed in the 16 GPa $< P <$ 25 GPa range where many phonon frequencies are imaginary and elastic moduli show large irregularities. Remarkably, as pressure is further increased above 50 GPa, the $Ia3d$ structure is shown to become stable again (all positive phonon frequencies and regular elastic constants).

Above approximately 15 GPa, a phase of $I\bar{4}3d$ symmetry (a non-centrosymmetric subgroup of $Ia3d$) is shown to become more stable than the $Ia3d$ one and to be elastically stable up to at least 60 GPa. In the 5 GPa $< P <$ 15 GPa pressure range, present *ab initio* calculations report clear thermodynamical instabilities of both phases, more so for $I\bar{4}3d$ than for $Ia3d$, thus suggesting two possible scenarios: i) the existence of a third phase or ii) a second order transition between the two phases.

Acknowledgements

The authors express their gratitude to Prof. Roberto Dovesi for his many valuable suggestions and to Dr. Javier Torres for helping in the preparation of Figure 1. AMNL acknowledges partial financial support by Conacyt - Mexico.

Notes and references

1 D. Griggs, Geophys. J. R. Astronom. Soc. **14**, 19 (1967).
2 R. Wilkins and W. Sabine, Am. Mineral. **58**, 508 (1973).
3 A. Beran and A. Putnis, Phys. Chem. Min. **9**, 57 (1983).
4 R. D. Aines and G. R. Rossman, Am. Mineral. **69**, 1116 (1984).
5 R. D. Aines and G. R. Rossman, J. Geophys. Res.: Solid Earth **89**, 4059 (1984).
6 F. Freund and G. Oberheuser, J. Geophys. Res.: Solid Earth **91**, 745 (1986).
7 G. R. Rossman, Min. Rev. Mineral. **18**, 193 (1988).
8 S. Mackwell, D. Kohlstedt, and M. Paterson, J. Geophys. Res.: Solid Earth (1978–2012) **90**, 11319 (1985).
9 E. Knittle, A. Hathorne, M. Davis, and Q. Williams, in *High-pressure research: application to Earth and planetary sciences*, edited by Y. Syono and M. H. Manghnani (American Geophysical Union, Washington D.C., 1992), pp. 297–304.
10 B. O'Neill, J. D. Bass, and G. R. Rossman, J. Geophys. Res.: Solid Earth **98**, 20031 (1993).
11 R. Nobes, E. Akhmatskaya, V. Milman, J. White, B. Winkler, and C. Pickard, Am. Mineral. **85**, 1706 (2000).
12 V. Milman, B. Winkler, R. Nobes, E. Akhmatskaya, C. Pickard, and J. White, JOM **52**, 22 (2000).
13 G. Lager, T. Armbruster, and J. Faber, Am. Mineral. **72**, 756 (1987).
14 H. Olijnyk, E. Paris, C. Geiger, and G. Lager, J. Geophys. Res.: Solid Earth **96**, 14313 (1991).
15 G. A. Lager and R. B. Von Dreele, Am. Mineral. **81**, 1097 (1996).
16 R. Nobes, E. Akhmatskaya, V. Milman, B. Winkler, and C. Pickard, Comput. Mat. Sci. **17**, 141 (2000).
17 G. A. Lager, R. T. Downs, M. Origlieri, and R. Garoutte, Am. Mineral. **87**, 642 (2002).
18 G. A. Lager, W. G. Marshall, Z. Liu, and R. T. Downs, Am. Mineral. **90**, 639 (2005).
19 F. Pertlik, GeoLines **15**, 113 (2003).
20 F. Pascale, P. Ugliengo, B. Civalleri, R. Orlando, Ph. D'Arco, and R. Dovesi, J. Chem. Phys. **121**, 1005 (2004).
21 R. Orlando, F. Torres, F. Pascale, P. Ugliengo, C. Zicovich-Wilson, and R. Dovesi, J. Phys. Chem. B **110**, 692 (2006).
22 R. M. Hazen and L. W. Finger, Am. Miner. **74**, 352 (1989).
23 A. D. Becke, J. Chem. Phys. **88**, 2547 (1988).
24 C. Lee, W. Yang, and R. G. Parr, Phys. Rev. B **37**, 785 (1988).
25 R. Dovesi, R. Orlando, A. Erba, C. M. Zicovich-Wilson, B. Civalleri, S. Casassa, L. Maschio, M. Ferrabone, M. De La Pierre, Ph. D'Arco, et al., Int. J. Quantum Chem. **114**, 1287 (2014).
26 R. Dovesi, V. R. Saunders, C. Roetti, R. Orlando, C. M. Zicovich-Wilson, F. Pascale, K. Doll, N. M. Harrison, B. Civalleri, I. J. Bush, et al., *CRYSTAL14 User's Manual*, Università di Torino, Torino (2014), http://www.crystal.unito.it.
27 K. Doll, Comput. Phys. Commun. **137**, 74 (2001).
28 K. Doll, V. Saunders, and N. Harrison, Int. J. Quantum Chem. **82**, 1 (2001).
29 B. Civalleri, Ph. D'Arco, R. Orlando, V. R. Saunders, and R. Dovesi, Chem. Phys. Lett. **348**, 131 (2001).
30 C. G. Broyden, IMA J. Appl. Math. **6**, 76 (1970).
31 R. Fletcher, Comput. J. **13**, 317 (1970).
32 D. Goldfarb, Mathematics of Computation **24**, 23 (1970).
33 D. F. Shanno, Mathematics of Computation **24**, 647 (1970).
34 K. Doll, Molecular Physics **108**, 223 (2010).
35 I. Souza and J. Martins, Phys. Rev. B **55**, 8733 (1997).
36 W. F. Perger, J. Criswell, B. Civalleri, and R. Dovesi, Comput. Phys. Commun. **180**, 1753 (2009).
37 A. Erba, A. Mahmoud, R. Orlando, and R. Dovesi, Phys. Chem. Miner. **41**, 151 (2014).
38 A. Erba, M. Ferrabone, J. Baima, R. Orlando, M. Rérat, and R. Dovesi, J. Chem. Phys. **138**, 054906 (2013).
39 A. Erba, K. E. El-Kelany, M. Ferrero, I. Baraille, and M. Rérat, Phys. Rev. B **88**, 035102 (2013).

40 A. Mahmoud, A. Erba, K. E. El-Kelany, M. Rérat, and R. Orlando, Phys. Rev. B **89**, 045103 (2014).
41 A. Erba and R. Dovesi, Phys. Rev. B **88**, 045121 (2013).
42 K. E. El-Kelany, A. Erba, P. Carbonnière, and M. Rérat, J. Phys.: Cond. Matter **26**, 205401 (2014).
43 J. Baima, A. Erba, R. Orlando, M. Rérat, and R. Dovesi, J. Phys. Chem. C **117**, 12864 (2013).
44 V. Lacivita, A. Erba, Y. Noël, R. Orlando, Ph. D'Arco, and R. Dovesi, J. Chem. Phys. **138**, 214706 (2013).
45 V. Lacivita, A. Erba, R. Dovesi, and Ph. D'Arco, Phys. Chem. Chem. Phys. **16**, 15331 (2014).
46 B. B. Karki, G. J. Ackland, and J. Crain, J. Phys.: Cond. Matter **9**, 8579 (1997).
47 J. Wang, J. Li, S. Yip, S. Phillpot, and D. Wolf, Phys. Rev. B **52**, 12627 (1995).
48 B. B. Karki, L. Stixrude, and R. M. Wentzcovitch, Rev. Geophys. **39**, 507 (2001).
49 D. C. Wallace, *Thermodynamics of Crystals* (Wiley, New York, USA, 1972).
50 D. C. Wallace, Rev. Mod. Phys. **37**, 57 (1965).
51 A. Erba, A. Mahmoud, D. Belmonte, and R. Dovesi, J. Chem. Phys. **140**, 124703 (2014).
52 A. Mahmoud, A. Erba, K. Doll, and R. Dovesi, J. Chem. Phys. **140**, 234703 (2014).
53 J. F. Nye, *Physical properties of crystals* (Oxford University Press, Oxford, 1957).
54 A. B. Alchagirov, J. P. Perdew, J. C. Boettger, R. C. Albers, and C. Fiolhais, Phys. Rev. B **63**, 224115 (2001).
55 R. E. Cohen, O. Gülseren, and R. J. Hemley, Am. Mineral. **85**, 338 (2000).
56 A. Erba, J. Chem. Phys. **141**, 124115 (2014).
57 F. D. Murnaghan, Proc. Natl. Acad. Sci. USA **30**, 244 (1944).
58 F. Birch, Phys. Rev. **71**, 809 (1947).
59 F. Birch, J. Geophys. Res. **83**, 1257 (1978).
60 P. Vinet, J. Ferrante, J. R. Smith, and J. H. Rose, J. Phys. C **19**, 467 (1986).
61 W. B. Holzapfel, Rep. Prog. Phys. **59**, 29 (1996).
62 J.-P. Poirier and A. Tarantola, Physics of the Earth and Planetary Interiors **109**, 1 (1998).
63 O. L. Anderson, *Equations of State of Solids for Geophysicists and Ceramic Science* (Oxford University Press, New York, 1995).
64 T. S. Duffy and Y. Wang, Mineralogical Society of America Reviews in Mineralogy **37**, 425 (1998).
65 J. Hama and K. Suito, J. Phys.: Cond. Matter **8**, 67 (1996).
66 F. Stacey, B. Brennan, and R. Irvine, Geophys. Surveys **4**, 189 (1981).
67 R. J. Angel, in *High-Pressure and High-Temperature Crystal Chemistry*, edited by R. Hazen and R. Downs (Mineralogical Society of America, 2000), pp. 35–59.
68 F. Pascale, C. M. Zicovich-Wilson, F. L. Gejo, B. Civalleri, R. Orlando, and R. Dovesi, J. Comp. Chem. **25**, 888 (2004).
69 C. M. Zicovich-Wilson, F. Pascale, C. Roetti, V. R. Saunders, R. Orlando, and R. Dovesi, J. Comp. Chem. **25**, 1873 (2004).
70 A. Erba, M. Ferrabone, R. Orlando, and R. Dovesi, J. Comput. Chem. **34**, 346 (2013).
71 C. Carteret, M. De La Pierre, M. Dossot, F. Pascale, A. Erba, and R. Dovesi, J. Chem. Phys. **138**, 014201 (2013).
72 J. M. Soler, E. Artacho, J. D. Gale, A. García, J. Junquera, P. Ordejón, and D. Sánchez-Portal, J. Phys.: Condens. Matter **14**, 2745 (2002).
73 G. Kresse and J. Furthmüller, Comput. Mat. Science **6**, 15 (1996).
74 G. Kresse and J. Furthmüller, Phys. Rev. B **54**, 11169 (1996).
75 Unfortunately, in the case of the $I\bar{4}3d$ phase of katoite, we could not establish the continuity of phonon modes on pressure due to high similarities among them and to a relatively small number of explored volumes.
76 Just to give an idea of the computational cost of this study, consider that the calculation of phonon frequencies of the $Ia3d$ phase takes about 5 hours when run in parallel on 640 CPUs (3200 CPU hours); the evaluation of elastic tensor takes about 7 hours on 640 CPUs (4480 CPU hours). A phonon frequency calculation for the $I\bar{4}3d$ phase takes about 7 hours on 1024 CPUs (7168 CPU hours). An elastic tensor calculation for the triclinic system, $P1$, requires about 31 hours on 640 CPUs (19840 CPU hours). Given that all calculations have been performed at several pressures (21 for EOS, 19, 7 and 8 for the elastic tensor of the $Ia3d$, $I\bar{4}3d$ and $P1$ phase, respectively, 9 and 6 for phonon calculations of $Ia3d$ and $I\bar{4}3d$ phases) and repeated a couple of times before finding the optimal setup, a total of about 1 million CPU hours have been used. All timings refer to the SuperMUC machine.